INTERNATIONAL JOURNAL FOR NUMERICAL METHODS IN ENGINEERING
Int. J. Numer. Meth. Engng 2007; **72**:1524–1543
Published online 27 March 2007 in Wiley InterScience (www.interscience.wiley.com). DOI: 10.1002/nme.2050

A linearly conforming point interpolation method (LC-PIM) for three-dimensional elasticity problems

G. Y. Zhang[1,*,†], G. R. Liu[1,2], Y. Y. Wang[3], H. T. Huang[4], Z. H. Zhong[5], G. Y. Li[5] and X. Han[5]

[1]*Department of Mechanical Engineering, Centre for Advanced Computations in Engineering Science (ACES), National University of Singapore, 9 Engineering Drive 1, Singapore 117576, Singapore*
[2]*The Singapore-MIT Alliance (SMA), E4-04-10, 4 Engineering Drive 3, Singapore 117576, Singapore*
[3]*Institute of High Performance Computing, Singapore, Singapore*
[4]*Six Tee Engineering Groups Pte Ltd, Singapore, Singapore*
[5]*State Key Laboratory of Advanced Technology for Vehicle Body Design and Manufacturing, Hunan University, Hunan, People's Republic of China*

SUMMARY

Linearly conforming point interpolation method (LC-PIM) is formulated for three-dimensional elasticity problems. In this method, shape functions are generated using point interpolation method by adopting polynomial basis functions and local supporting nodes are selected based on the background cells. The shape functions so constructed have the Kronecker delta functions property and it allows straightforward imposition of point essential boundary conditions. Galerkin weak form is used for creating discretized system equations, and a nodal integration scheme with strain-smoothing operation is used to perform the numerical integration. The present LC-PIM can guarantee linear exactness and monotonic convergence for the numerical results. Numerical examples are used to examine the present method in terms of accuracy, convergence, and efficiency. Compared with the finite element method using linear elements, the LC-PIM can achieve better efficiency, and higher accuracy especially for stresses. Copyright © 2007 John Wiley & Sons, Ltd.

Received 9 August 2006; Revised 6 January 2007; Accepted 19 February 2007

KEY WORDS: mesh free; linearly conforming; point interpolation method; nodal integration; three dimensional

*Correspondence to: G. Y. Zhang, Department of Mechanical Engineering, Centre for Advanced Computations in Engineering Science (ACES), National University of Singapore, 9 Engineering Drive 1, Singapore 117576, Singapore.
†E-mail: g0203729@nus.edu.sg

1. INTRODUCTION

Mesh-free methods have been proposed and achieve remarkable progress in recent years, such as the smooth particle hydrodynamic method [1, 2], general finite difference method [3], the diffuse element method [4], the element-free Galerkin method [5], reproducing kernel particle methods [6] and the meshless local Petrov–Galerkin method [7], etc.

The point interpolation method (PIM) is a mesh-free method based on Galerkin weak form. In this method, the shape functions are constructed using simple interpolation through a set of nodes located in a local support domain. For different basis functions adopted, two types of PIM have been developed, i.e. polynomial PIM using polynomial basis functions [8–10] and radial PIM (RPIM) using radial basis functions [11, 12]. In the original PIMs, Gauss integration scheme is used to perform the numerical integration. Although both these two methods can provide linear consistent shape functions, neither of them could guarantee a linear exactness of the solutions due to the inconformability or incompatibility.

Recently, a scheme of stabilized conforming nodal integration has been proposed by Chen and coworkers [13]. In their works, the technique of strain smoothing is introduced in order to eliminate the error in the procedure of direct nodal integration. By using the stabilized conforming nodal integration scheme, the integration constraints can be met and linear exactness in the solution can be guaranteed based on the linear consistent shape functions [13]. Liu *et al.* have applied the scheme of nodal integration into the original PIMs, linearly conforming PIM (LC-PIM) [14] and linearly conforming RPIM (LC-RPIM) [15] have been formulated for 2-D elastic problems and shown good performance.

In this paper, the LC-PIM is extended for 3-D problems. In this method, a background cell of four-node tetrahedrons is employed and shape functions are constructed using linear polynomials, as tetrahedrons can be created by standard routines automatically for 3-D solids. The stabilized nodal integration scheme with strain smoothing is extended to 3-D problems and volume integrals involving shape function gradients are recast into surface integrals involving only shape functions. The present method so constructed can guarantee the linear exactness of the numerical solution and is computationally efficient.

2. POINT INTERPOLATION METHOD

In the present method, polynomials are used to serve as basis functions to create shape functions. Consider a continuous function $u(\mathbf{x})$, which is a displacement component for our solid mechanics problems. It can be approximated in the vicinity of $\mathbf{x}$ as follows:

$$u(\mathbf{x}) = \sum_{i=1}^{n} p_i(\mathbf{x}) a_i = \mathbf{p}^{\mathrm{T}}(\mathbf{x})\mathbf{a} \tag{1}$$

where $p_i(\mathbf{x})$ is polynomial basis function of $\mathbf{x} = [x, y, z]^{\mathrm{T}}$, n is the number of polynomial terms, and $\mathbf{a} = \{a_1, a_2, \ldots, a_n\}^{\mathrm{T}}$, in which a_i is the corresponding coefficient yet to be determined. The polynomial basis $p_i(\mathbf{x})$ is usually built utilizing the Pascal's triangles, and a complete basis is preferred because of the requirement of higher possible order of consistency. The complete polynomial basis of order 1 and order 2 in three dimensions can be written in the

DOI: 10.1002/nme

following forms:

$$\begin{aligned} \mathbf{p}^{\mathrm{T}}(\mathbf{x}) &= \{1 \;\; x \;\; y \;\; z\} && \text{Bases of complete 1st order} \\ \mathbf{p}^{\mathrm{T}}(\mathbf{x}) &= \{1 \;\; x \;\; y \;\; z \;\; x^2 \;\; y^2 \;\; z^2 \;\; xy \;\; yz \;\; zx\} && \text{Bases of complete 2nd order} \end{aligned} \tag{2}$$

The coefficients $\mathbf{a}$ in Equation (1) can then be determined by enforcing $u(\mathbf{x})$ to be the nodal displacements at these n nodes in the support domain of $\mathbf{x}$, which would lead to the following n equations:

$$\begin{aligned} u(x_1, y_1, z_1) &= a_1 + a_2 x_1 + a_3 y_1 + a_4 z_1 + \cdots + a_n p_n(\mathbf{x}_1) \\ u(x_2, y_2, z_2) &= a_1 + a_2 x_2 + a_3 y_2 + a_4 z_2 + \cdots + a_n p_n(\mathbf{x}_2) \\ &\vdots \\ u(x_n, y_n, z_n) &= a_1 + a_2 x_n + a_3 y_n + a_4 z_n + \cdots + a_n p_n(\mathbf{x}_n) \end{aligned} \tag{3}$$

In matrix form, it can be written as

$$\mathbf{U}_{\mathrm{s}} = \mathbf{P}_n \mathbf{a} \tag{4}$$

where $\mathbf{U}_{\mathrm{s}}$ is the vector of nodal displacements in the support domain

$$\mathbf{U}_{\mathrm{s}} = \{u_1 \;\; u_2 \;\; u_3 \;\; \ldots \;\; u_n\}^{\mathrm{T}} \tag{5}$$

$\mathbf{P}_n$ the polynomial moment matrix given by

$$\mathbf{P}_n = \begin{bmatrix} 1 & x_1 & y_1 & z_1 & \ldots & p_n(\mathbf{x}_1) \\ 1 & x_2 & y_2 & z_2 & \ldots & p_n(\mathbf{x}_2) \\ 1 & x_3 & y_3 & z_3 & \ldots & p_n(\mathbf{x}_3) \\ \vdots & \vdots & \vdots & \vdots & \ddots & \vdots \\ 1 & x_n & y_n & z_n & \ldots & p_n(\mathbf{x}_n) \end{bmatrix} \tag{6}$$

Assuming the existence of $\mathbf{P}_n^{-1}$, a unique solution for $\mathbf{a}$ can be obtained as

$$\mathbf{a} = \mathbf{P}_n^{-1} \mathbf{U}_{\mathrm{s}} \tag{7}$$

Substituting Equation (7) back into Equation (1) yields

$$u(\mathbf{x}) = \mathbf{P}^{\mathrm{T}}(\mathbf{x}) \mathbf{P}_n^{-1} \mathbf{U}_{\mathrm{s}} = \sum_{i=1}^{n} \varphi_i u_i = \boldsymbol{\Phi}^{\mathrm{T}}(\mathbf{x}) \mathbf{U}_{\mathrm{s}} \tag{8}$$

where $\boldsymbol{\Phi}(\mathbf{x})$ is the vector of PIM shape functions

$$\boldsymbol{\Phi}^{\mathrm{T}}(\mathbf{x}) = \{\varphi_1(\mathbf{x}) \;\; \varphi_2(\mathbf{x}) \;\; \ldots \;\; \varphi_n(\mathbf{x})\} \tag{9}$$

The kth derivative of the shape functions can be easily obtained, but they are not required in our LC-PIM formulations due to the use of strain-smoothing operation to be described in Section 3.

DOI: 10.1002/nme

In the present method, linear monomials are used to serve as the basis functions. Similarly, as in the finite element method (FEM), four vertexes of the background four-node tetrahedron cell are taken to perform the interpolation of the interest points located inside the cell. This can be easily implemented and can always ensure the invertability of the moment matrix, as long as the four vertexes of the tetrahedron are not on a plane.

3. NODAL INTEGRATION OF WEAK FORM

3.1. Galerkin weak form

Consider a 3-D solid mechanics problem defined in domain Ω bounded by Γ, which can be expressed by the following equations [16].

Equilibrium equation:

$$\mathbf{L}^{\mathrm{T}}\boldsymbol{\sigma} + \mathbf{b} = 0 \quad \text{in } \Omega \tag{10}$$

where $\mathbf{L}$ is a differential operator in the following form:

$$\mathbf{L}^{\mathrm{T}} = \begin{bmatrix} \dfrac{\partial}{\partial x} & 0 & 0 & \dfrac{\partial}{\partial y} & 0 & \dfrac{\partial}{\partial z} \\ 0 & \dfrac{\partial}{\partial y} & 0 & \dfrac{\partial}{\partial x} & \dfrac{\partial}{\partial z} & 0 \\ 0 & 0 & \dfrac{\partial}{\partial z} & 0 & \dfrac{\partial}{\partial y} & \dfrac{\partial}{\partial x} \end{bmatrix} \tag{11}$$

$\boldsymbol{\sigma}^{\mathrm{T}} = \{\sigma_{xx} \ \sigma_{yy} \ \sigma_{zz} \ \sigma_{xy} \ \sigma_{yz} \ \sigma_{zx}\}$ is the stress vector, $\mathbf{u}^{\mathrm{T}} = \{u \ v \ w\}$ is the displacement vector, and $\mathbf{b}^{\mathrm{T}} = \{b_x \ b_y \ b_z\}$ is the body force vector.

Essential boundary conditions:

$$\mathbf{u} = \bar{\mathbf{u}} \quad \text{on } \Gamma_u \tag{12}$$

where $\bar{\mathbf{u}}$ is the prescribed displacement on the essential boundaries.

Natural boundary conditions:

$$\boldsymbol{\sigma} \cdot \mathbf{n} = \bar{\mathbf{t}} \quad \text{on } \Gamma_t \tag{13}$$

where $\bar{\mathbf{t}}$ is the prescribed traction on the natural boundaries, and $\mathbf{n}$ is the vector of unit outward normal. Note that $\Gamma = \Gamma_u + \Gamma_t$.

The standard Galerkin weak form for this problem can be expressed as

$$\int_{\Omega} (\mathbf{L}\delta\mathbf{u})^{\mathrm{T}} (\mathbf{D}\mathbf{L}\mathbf{u}) \, \mathrm{d}\Omega - \int_{\Omega} \delta\mathbf{u}^{\mathrm{T}}\mathbf{b} \, \mathrm{d}\Omega - \int_{\Gamma_t} \delta\mathbf{u}^{\mathrm{T}}\bar{\mathbf{t}} \, \mathrm{d}\Gamma = 0 \tag{14}$$

where $\mathbf{D}$ is the matrix of material constants.

Substituting Equation (8) into Equation (14), the discretized system equation can be expressed in the following matrix form:

$$\mathbf{K}\mathbf{u} = \mathbf{f} \tag{15}$$

DOI: 10.1002/nme

where

$$\mathbf{K}_{ij} = \int_{\Omega} \mathbf{B}_i^{\mathrm{T}} \mathbf{D} \mathbf{B}_j \, \mathrm{d}\Omega \tag{16}$$

$$\mathbf{f}_i = \int_{\Gamma_t} \varphi_i \bar{\mathbf{t}} \, \mathrm{d}\Gamma + \int_{\Omega} \varphi_i \mathbf{b} \, \mathrm{d}\Omega \tag{17}$$

$$\mathbf{B}_i = \begin{bmatrix} \varphi_{i,x} & 0 & 0 \\ 0 & \varphi_{i,y} & 0 \\ 0 & 0 & \varphi_{i,z} \\ \varphi_{i,y} & \varphi_{i,x} & 0 \\ 0 & \varphi_{i,z} & \varphi_{i,y} \\ \varphi_{i,z} & 0 & \varphi_{i,x} \end{bmatrix} \tag{18}$$

3.2. Nodal integration scheme with strain-smoothing operation

To carry out the domain integration in Equations (16) and (17), several types of numerical integration schemes can be used. For example, the Gauss integration scheme is widely adopted in the process of numerical integration. In the present method, the nodal integration scheme with strain-smoothing operation [13] is adopted to perform the integration.

In the process of nodal integration, a background cell of four-node tetrahedrons is needed, and it can be generated easily using any mesh generator developed for FEM. Afterwards, the problem domain Ω will be divided into N smoothing domains Ω_k $(k = 1, \ldots, N)$, in which N is the total number of field nodes. The smoothing domain for each field node is centred by the node and constructed based on the background cells of four-node tetrahedrons. As illustrated in Figure 1, the sub-domain of the smoothing domain for node k located in the particular cell j can be obtained by connecting the mid-edge-points, the centroids of the surface triangles, and the centroid of cell j. Finding out other sub-domains located in cells which contain node k and the smoothing domain for node k can be constructed by uniting all the sub-domains.

Applying the nodal integration scheme, the domain integration can be performed numerically as follows:

$$\mathbf{K}_{ij} = \sum_{k=1}^{N} \mathbf{K}_{ij}^{(k)} \tag{19}$$

in which

$$\mathbf{K}_{ij}^{(k)} = \int_{\Omega_k} \mathbf{B}_i^{\mathrm{T}} \mathbf{D} \mathbf{B}_j \, \mathrm{d}\Omega \tag{20}$$

DOI: 10.1002/nme

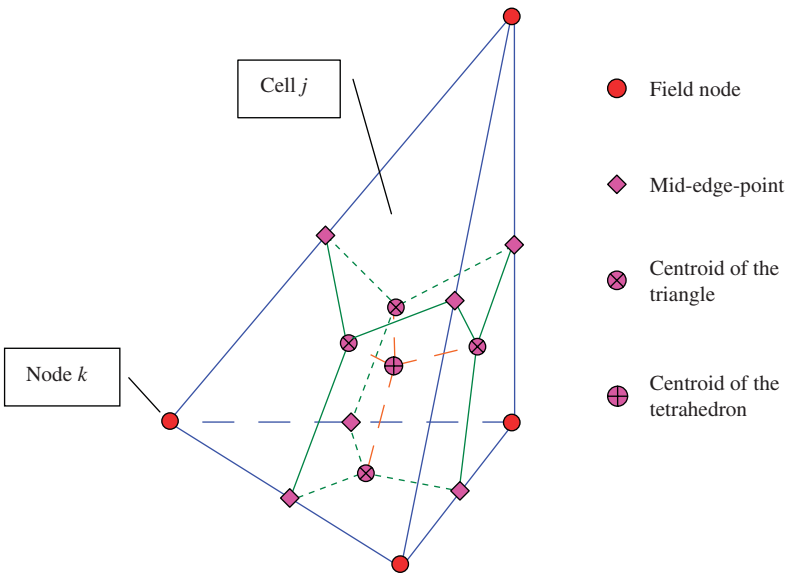

Figure 1. Illustration of background four-node tetrahedron cell and one of the subsmoothing-domain for node k located in cell j created by connecting the mid-edge-points, the centroids of the surface triangles and the centroid of the tetrahedron.

In the present method, to guarantee a linear exactness in the solution, a technique of smoothing is applied on the strains [13]

$$\tilde{\varepsilon}_{ij}^{h}(\mathbf{x}_k) = \int_{\Omega_k} \varepsilon_{ij}^{h}(\mathbf{x}) \Psi(\mathbf{x} - \mathbf{x}_k)\, \mathrm{d}\Omega \tag{21}$$

where Ψ is a smoothing function.

For simplicity, we use

$$\Psi(\mathbf{x} - \mathbf{x}_k) = \begin{cases} 1/V_k, & \mathbf{x} \in V_k \\ 0, & \mathbf{x} \notin V_k \end{cases} \tag{22}$$

where $V_k = \int_{\Omega_k} \mathrm{d}\Omega$ is the volume of the smoothing domain for node k.

Substituting Equation (22) into Equation (21) and integrating by parts, we obtain

$$\begin{aligned} \tilde{\varepsilon}_{ij}^{h}(\mathbf{x}_k) &= \frac{1}{V_k} \int_{\Omega_k} \varepsilon_{ij}^{h}(\mathbf{x})\, \mathrm{d}\Omega \\ &= \frac{1}{V_k} \int_{\Omega_k} \frac{1}{2} \left(\frac{\partial u_i^h}{\partial x_j} + \frac{\partial u_j^h}{\partial x_i} \right) \mathrm{d}\Omega \\ &= \frac{1}{2V_k} \int_{\Gamma_k} (u_i^h n_j + u_j^h n_i)\, \mathrm{d}\Gamma \end{aligned} \tag{23}$$

DOI: 10.1002/nme

where Γ_k is the boundary surface of the smoothing domain for node k. Introducing the PIM shape functions into Equation (23), the smoothed strain can be written in the following matrix form:

$$\tilde{\boldsymbol{\varepsilon}}^h(\mathbf{x}_k) = \sum_{i \in G_k} \tilde{\mathbf{B}}_i(\mathbf{x}_k)\mathbf{U}_i \tag{24}$$

where G_k contains a number of nodes whose shape functions support cover node k. In 3-D space

$$\tilde{\boldsymbol{\varepsilon}}^{h\mathrm{T}} = \{\tilde{\varepsilon}^h_{xx} \;\; \tilde{\varepsilon}^h_{yy} \;\; \tilde{\varepsilon}^h_{zz} \;\; \tilde{\varepsilon}^h_{xy} \;\; \tilde{\varepsilon}^h_{yz} \;\; \tilde{\varepsilon}^h_{zx}\}, \quad \mathbf{U}_i^{\mathrm{T}} = \{u_{xi} \;\; u_{yi} \;\; u_{zi}\} \tag{25}$$

$$\tilde{\mathbf{B}}_i(\mathbf{x}_k) = \begin{bmatrix} \tilde{b}_{ix}(\mathbf{x}_k) & 0 & 0 \\ 0 & \tilde{b}_{iy}(\mathbf{x}_k) & 0 \\ 0 & 0 & \tilde{b}_{iz}(\mathbf{x}_k) \\ \tilde{b}_{iy}(\mathbf{x}_k) & \tilde{b}_{ix}(\mathbf{x}_k) & 0 \\ 0 & \tilde{b}_{iz}(\mathbf{x}_k) & \tilde{b}_{iy}(\mathbf{x}_k) \\ \tilde{b}_{iz}(\mathbf{x}_k) & 0 & \tilde{b}_{ix}(\mathbf{x}_k) \end{bmatrix} \tag{26}$$

$$\tilde{b}_{il} = \frac{1}{V_k}\int_{\Omega_k} \varphi_i(\mathbf{x}) n_l(\mathbf{x})\, \mathrm{d}\Omega \quad (l = x, y, z) \tag{27}$$

Applying Gauss integration among each part of the surface Γ_k of smoothing domain Ω_k, the above equation can be written in algebraic form as

$$\tilde{b}_{il} = \frac{1}{V_k}\sum_{m=1}^{N_\mathrm{s}} \left[\sum_{n=1}^{N_\mathrm{g}} w_n(\varphi_i(\mathbf{x}_{mn}) n_l(\mathbf{x}_m)) \right] \tag{28}$$

where N_s is the number of surface areas of smoothing domain Ω_k, N_g is the number of Gauss points distributed in each area, and w_n is the corresponding weight number of Gauss integration scheme. In the present method, $N_\mathrm{g} = 4$ is adopted which means that 2×2 Gauss points are used for integration on each quadrangular surface area of the smoothing domain.

It has been shown that the strain smoothing can successfully eliminate spatial instability in nodal integration. Furthermore, the employment of the nodal integration scheme together with the linearly consistent shape functions in Galerkin weak form can guarantee a linear exactness in the numerical solutions [13]. All these properties will be demonstrated numerically using the following examples.

4. NUMERICAL RESULTS

Several numerical examples are reported in this section. The error indicators in displacement and energy are, respectively, defined as follows:

$$e_\mathrm{d} = \sqrt{\frac{\sum_{i=1}^{n} (u_i^{\mathrm{exact}} - u_i^{\mathrm{numerical}})^2}{\sum_{i=1}^{n} (u_i^{\mathrm{exact}})^2}} \tag{29}$$

DOI: 10.1002/nme

Table I. Displacement error of the linear patch.

Location of node 9	(5, 5, 5)	(9.9, 9.9, 9.9)	(9.9, 9.9, 0.1)	(0.1, 5, 5)	(5, 5, 0.1)
Error in displacement	2.5807E−16	2.0467D−14	1.4951D−14	2.4072D−16	1.5590D−16

$$e_{\mathrm{e}}=\frac{1}{V}\sqrt{\frac{1}{2}\int_{\Omega}(\boldsymbol{\varepsilon}^{\mathrm{exact}}-\boldsymbol{\varepsilon}^{\mathrm{numerical}})^{\mathrm{T}}\mathbf{D}(\boldsymbol{\varepsilon}^{\mathrm{exact}}-\boldsymbol{\varepsilon}^{\mathrm{numerical}})\,\mathrm{d}\Omega} \tag{30}$$

where the superscript *exact* notes the exact or analytical solution, *numerical* notes a numerical solution obtained using a numerical method including the present LC-PIM, and V is the volume of the problem domain.

4.1. Standard patch test

For a numerical method working for solid mechanics problems, the sufficient requirement for convergence is to pass the standard patch test [17]. Therefore, the first example is the standard patch test using the present LC-PIM. The problem is studied in a cubic domain with the dimension of $10\times10\times10$, and the displacements are prescribed on all outside boundaries by the following linear function:

$$\begin{aligned} u_x &= 0.6x \\ u_y &= 0.6y \\ u_z &= 0.6z \end{aligned} \tag{31}$$

The linear patch test is first conducted using a set of nodes distributed in the cubic domain, i.e. eight nodes locate on the vertexes of the cube and the ninth node locates inside. By changing the location of the ninth node inside the cube, displacement error as defined in Equation (29) has been calculated and listed in Table I. It can be found that the present method can pass the linear patch test regardless the location of the ninth node. This result numerically proves the stability of the LC-PIM.

Second, the problem domain has been represented using both 125 regularly and 166 irregularly distributed nodes as shown in Figure 2. For these two models, the errors in displacement are found to be 1.2837×10^{-15} and 1.2036×10^{-15}, respectively, which reach almost the level of the machine precision. The results show that the displacements of all the interior nodes follow 'exactly' the same function of the imposed displacement. This example demonstrates numerically that the present LC-PIM can monotonically converge due to its ability to reproduce linear fields and the use of the Galerkin weak form.

4.2. Cantilever beam

The performance of the present method is evaluated using the cantilever beam problem under a parabolic traction on the right edge. As shown in Figure 3, the beam is of $L=10\,\mathrm{m}$, $H=1\,\mathrm{m}$, $B=1\,\mathrm{m}$, and $P=-100\,\mathrm{N}$. The relative parameters are taken as $E=3.0\times10^{7}\,\mathrm{kPa}$ and $v=0.3$. Since the beam is relatively thin, analytical solution based on the plane stress theory can be used

DOI: 10.1002/nme

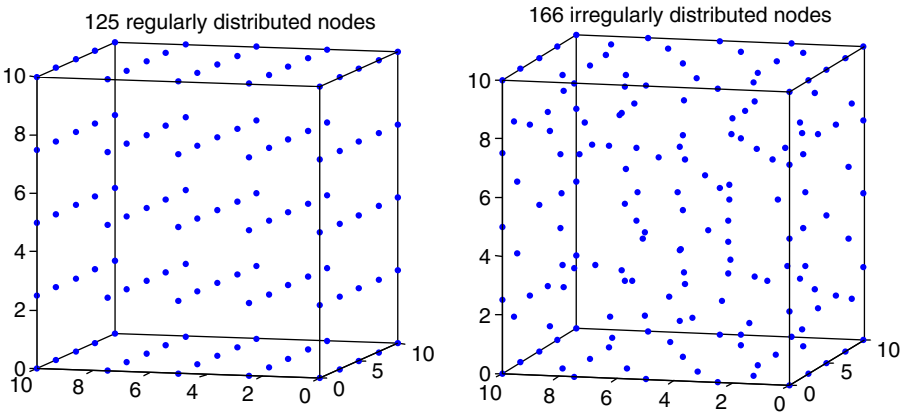

Figure 2. Illustration of nodal distributions of a cube for the standard patch test.

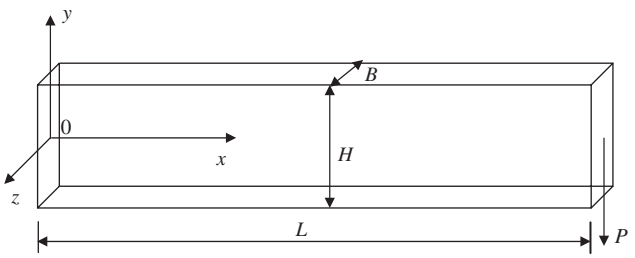

Figure 3. 3-D cantilever beam subjected to a parabolic traction on the right edge.

approximately as reference solutions [16]

$$u_x = -\frac{Py}{6EI}\left[(6L-3x)x + (2+v)\left(y^2 - \frac{H^2}{4}\right)\right] \tag{32}$$

$$u_y = \frac{P}{6EI}\left[3vy^2(L-x) + (4+5v)\frac{H^2x}{4} + (3L-x)x^2\right] \tag{33}$$

$$\sigma_x = -\frac{P(L-x)y}{I} \tag{34}$$

$$\sigma_y = 0 \tag{35}$$

$$\sigma_{xy} = \frac{P}{2I}\left[\frac{H^2}{4} - y^2\right] \tag{36}$$

where I is the moment of inertia given as $I = H^3/12$.

DOI: 10.1002/nme

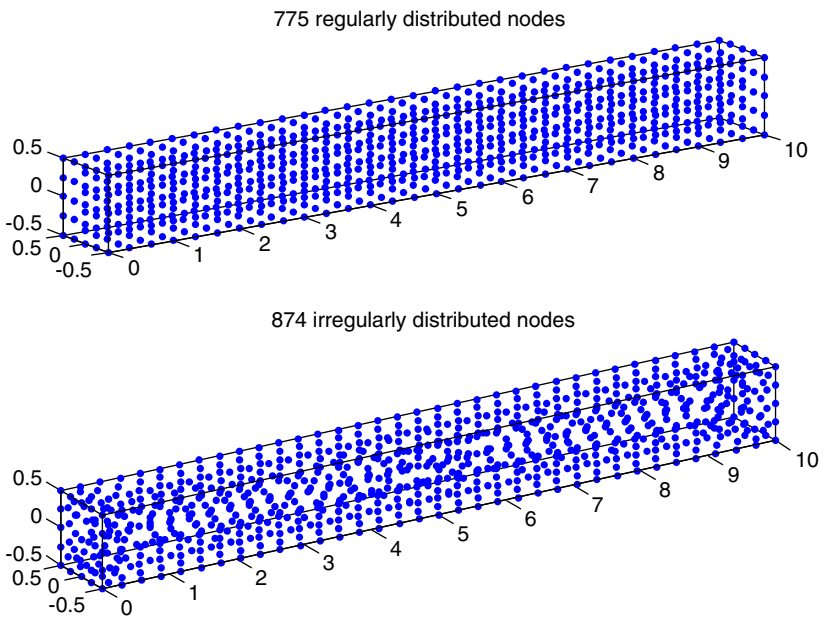

Figure 4. Illustration of nodal distributions of the 3-D cantilever beam.

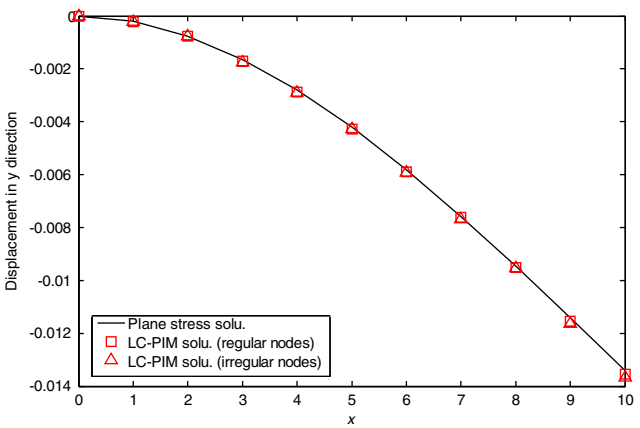

Figure 5. Deflection distribution along the neutral line of the 3-D cantilever beam.

The problem domain is presented using both 775 regularly and 874 irregularly distributed nodes (as shown in Figure 4), and computed distribution of defection along the neutral line and shear stress (τ_{xy}) along the mid-line ($x = L/2$, $z = 0$) are plotted together with the reference solutions in Figures 5 and 6, respectively. It can be found that the numerical results obtained using the present LC-PIM with both regular and irregular nodal distribution models are in very good agreement with the reference ones.

DOI: 10.1002/nme

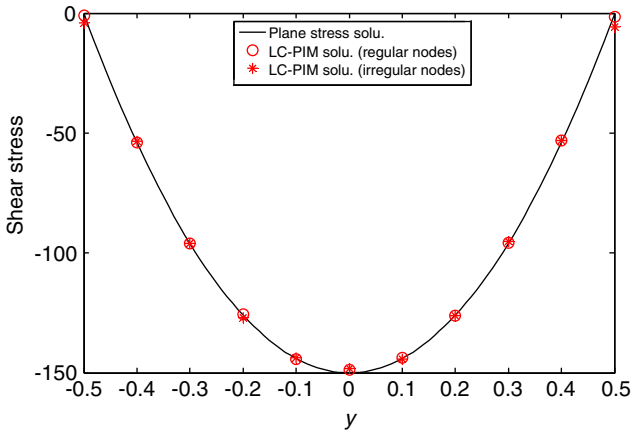

Figure 6. Shear stress distribution along the line of $(x = L/2, z = 0)$ of the 3-D cantilever beam.

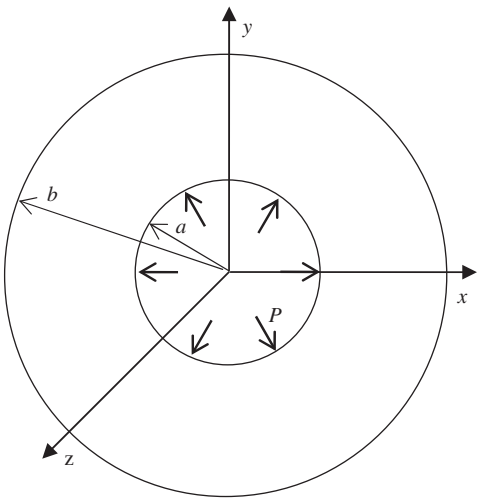

Figure 7. The Lame problem of a hollow sphere under internal pressure.

4.3. 3-D Lame problem

The 3-D Lame problem consists of a hollow sphere with inner radius a and outer radius b and subjected to internal pressure P, as shown in Figure 7. For this benchmark problem, the analytical solution is available in polar co-ordinate system [16]

$$u_r = \frac{Pa^3 r}{E(b^3 - a^3)} \left[(1 - 2\nu) + (1 + \nu) \frac{b^3}{2r^3} \right] \tag{37}$$

DOI: 10.1002/nme

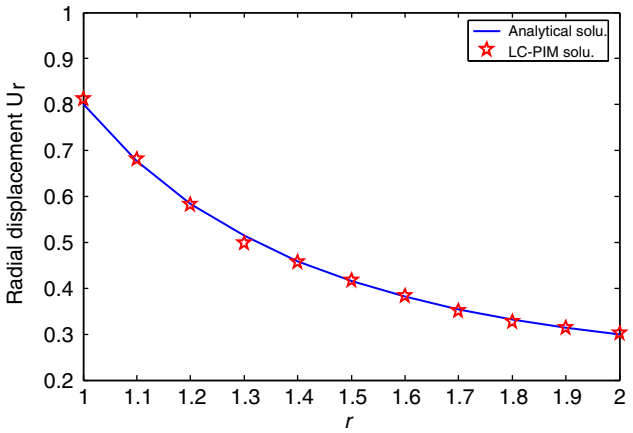

Figure 8. Distribution of the radial displacement along the x-axis for the 3-D Lame problem.

$$\sigma_r = \frac{Pa^3(b^3 - r^3)}{r^3(a^3 - b^3)} \tag{38}$$

$$\sigma_\theta = \frac{Pa^3(b^3 + 2r^3)}{2r^3(b^3 - a^3)} \tag{39}$$

where r is the radial distance form the centroid of the sphere to the point of interest in the sphere.

As the problem is spherically symmetrical, only one-eighth of the sphere is modelled and symmetry conditions are imposed on the three planes of symmetry. The numerical solution of this problem has been calculated using the material parameters $E = 1.0\,\text{kPa}$, $v = 0.3$, geometric parameters $a = 1\,\text{m}$, $b = 2\,\text{m}$ and internal pressure $P = 1\,\text{N/m}^2$. The problem domain is presented using 1304 irregularly distributed nodes. The computed nodal displacements and stresses along the x-axis are plotted in Figures 8 and 9, respectively. It can be clearly seen that the numerical results agree well with the analytical ones.

Furthermore, to investigate the properties of convergence and efficiency of the present LC-PIM, four models of 173, 317, 729, and 1304 irregularly distributed nodes are employed. For each model of nodes distribution, the error in energy of the numerical results is calculated according to the definition in Equation (30). For comparison, the FEM using linear four-node tetrahedron element is also employed to study the problem with the same nodes distributions. As shown in Figure 10, the results of error in energy norm against h are plotted for both the FEM and the present LC-PIM, where h is the average nodal spacing of the nodes distribution. It is found obviously that these two methods reach similar rates of convergence, but the LC-PIM obtains more accurate results compared with the linear FEM. In Figure 11, the energy errors of the numerical results obtained using these two methods are plotted against the central processing unit time consumed, which shows performance of numerical methods. It can be found that the LC-PIM is clearly more efficient than the linear FEM.

DOI: 10.1002/nme

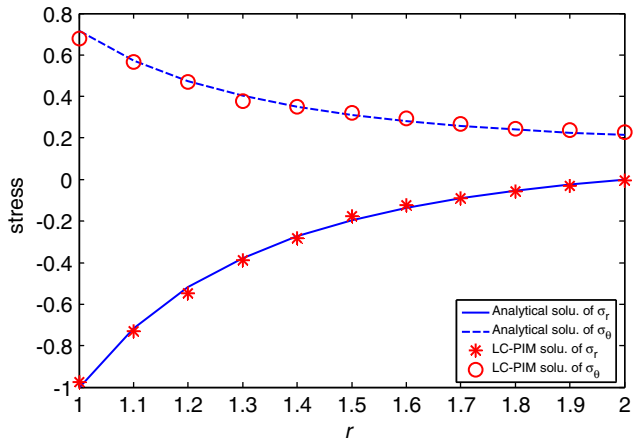

Figure 9. Distribution of radial and tangential stresses along the x-axis for the 3-D Lame problem.

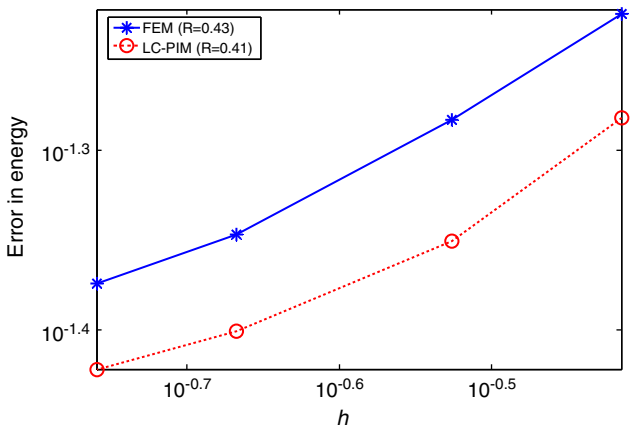

Figure 10. Comparison of convergence between FEM and LC-PIM *via* the Lame problem with the same nodes distribution.

4.4. 3-D Kirsch problem

The 3-D Kirsch problem is considered to examine the stress distribution in the vicinity of a small cavity in an infinite cube subjected to far-field uniform tension, as illustrated in Figure 12. The analytical solution for the normal stress (σ_{zz}) in the plane $z=0$ is given as [16]

$$\sigma_{zz} = \sigma_0 \left[1 + \frac{4-5v}{2(7-5v)} \left(\frac{a}{r}\right)^3 + \frac{9}{2(7-5v)} \left(\frac{a}{r}\right)^5 \right] \tag{40}$$

where r is the radial distance from the centroid of the cube to the point of interest.

DOI: 10.1002/nme

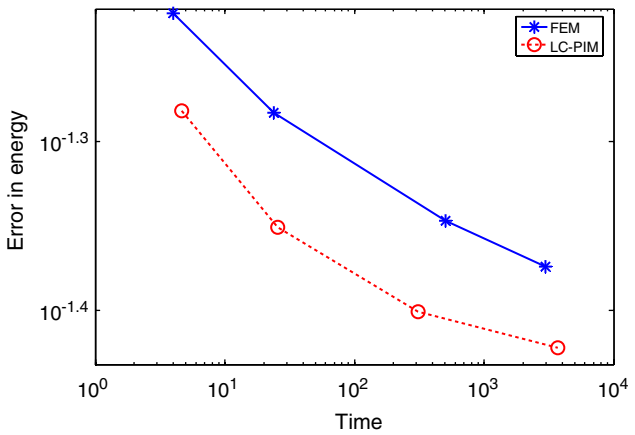

Figure 11. Comparison of efficiency between FEM and LC-PIM *via* the Lame problem with the same nodes distribution.

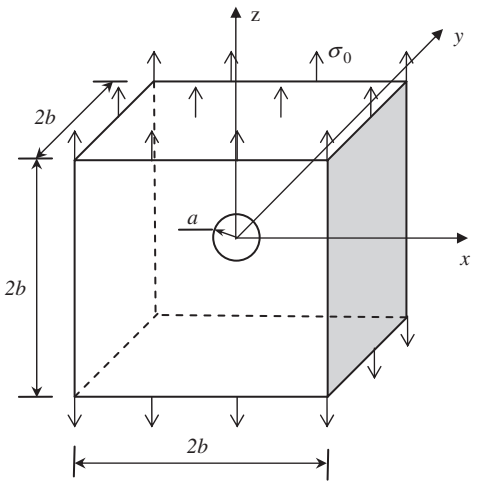

Figure 12. 3-D Kirsch problem: a cube with a spherical cavity subjected to a uniform tension.

The problem is modelled for $a = 1\,\text{m}$, $b = 10\,\text{m}$ and $\sigma_0 = 1\,\text{N/m}^2$ with the material parameters, $E = 3.0 \times 10^7\,\text{kPa}$ and $v = 0.3$. The problem domain is presented with total 1256 nodes. Figure 13 shows the comparison between the analytical solution and the numerical solution for the normal stress σ_{zz} along the x-axis. It can be clearly seen again that the LC-PIM solution is in excellent agreement with the analytical ones.

DOI: 10.1002/nme

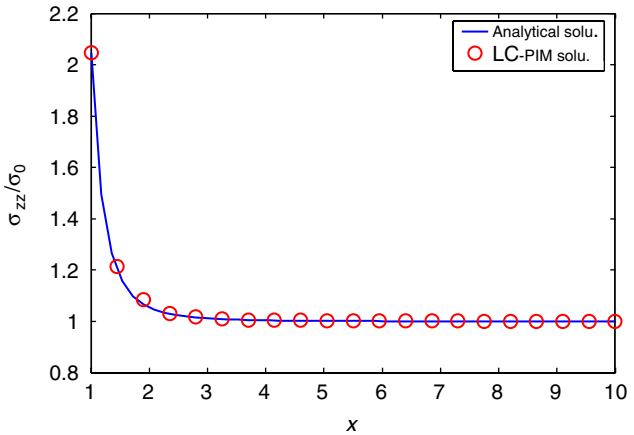

Figure 13. Distribution of σ_{zz} along the x-axis for the Kirsch problem.

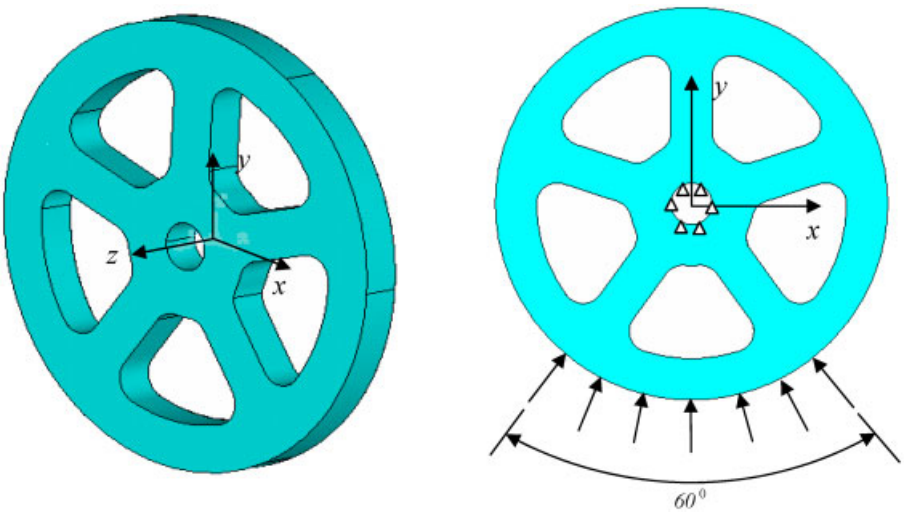

Figure 14. Simplified model of an automotive rim.

4.5. An automotive part: rim

A typical rim used in automotive industry is modelled and studied using the present method. As shown in Figure 14, the rim is of inner radius 2 m, outer radius 19 m and a thickness of 3 m. It is constrained in three dimensions along the inner annulus and a uniform pressure of 100 N/m^2 is applied on the outer annulus of 60°. As no analytical solution is available for this problem, a reference solution is obtained using the FEM software NASTRAN, in which a very fine mesh is adopted. The problem domain is represented using 7972 nodes and the numerical solutions

DOI: 10.1002/nme

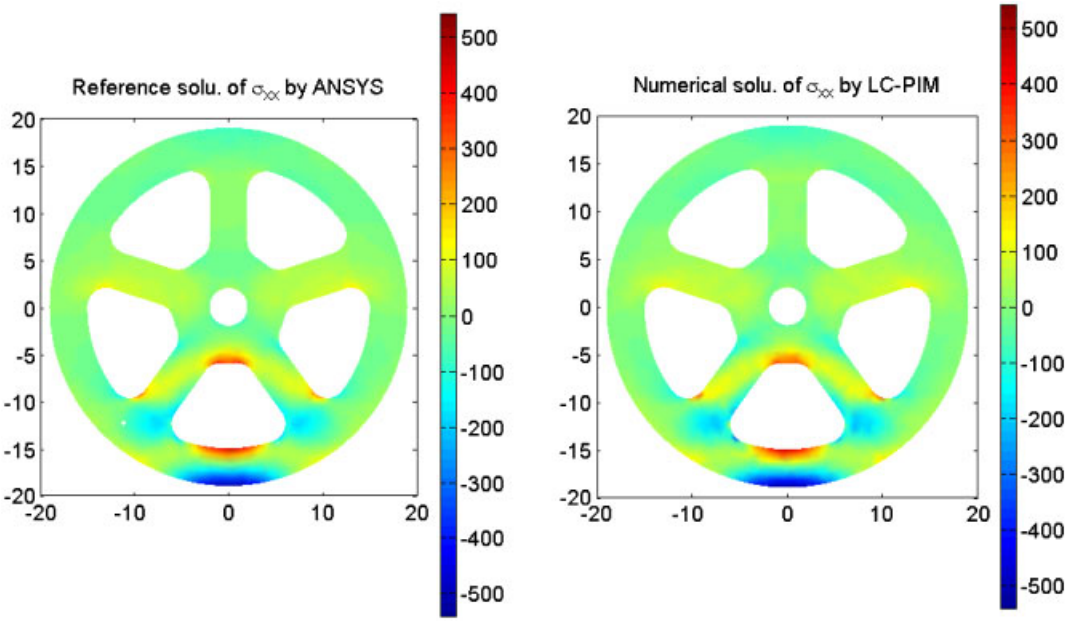

Figure 15. Stress contour of σ_{xx} on the plane $z = 0$ for the rim problem.

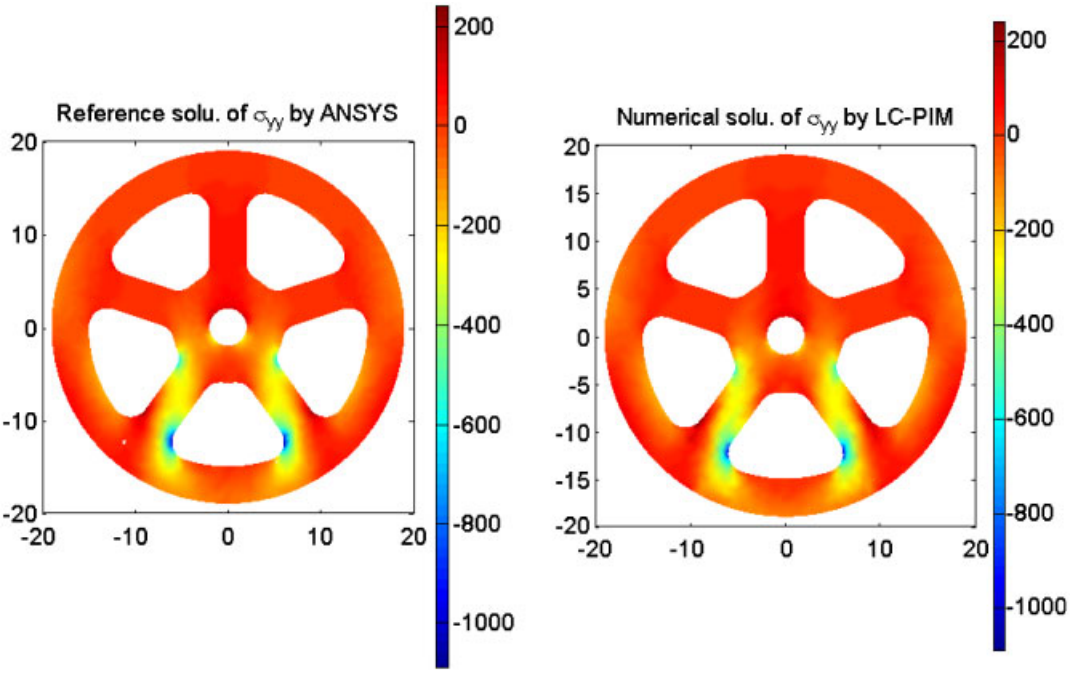

Figure 16. Stress contour of σ_{yy} on the plane $z = 0$ for the rim problem.

DOI: 10.1002/nme

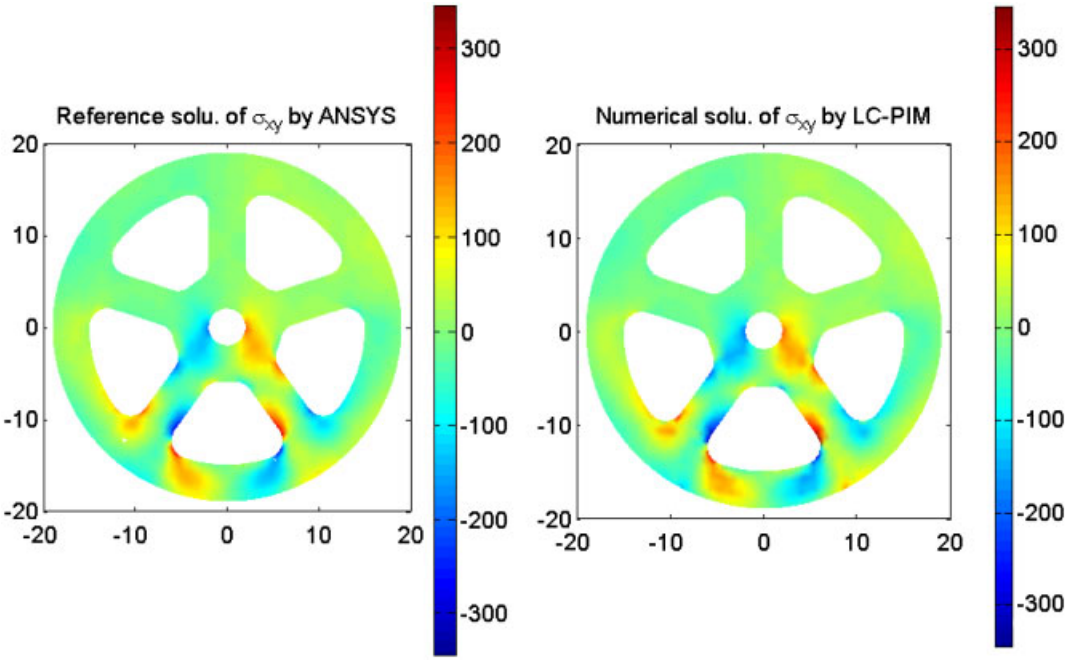

Figure 17. Stress contour of σ_{xy} on the plane $z = 0$ for the rim problem.

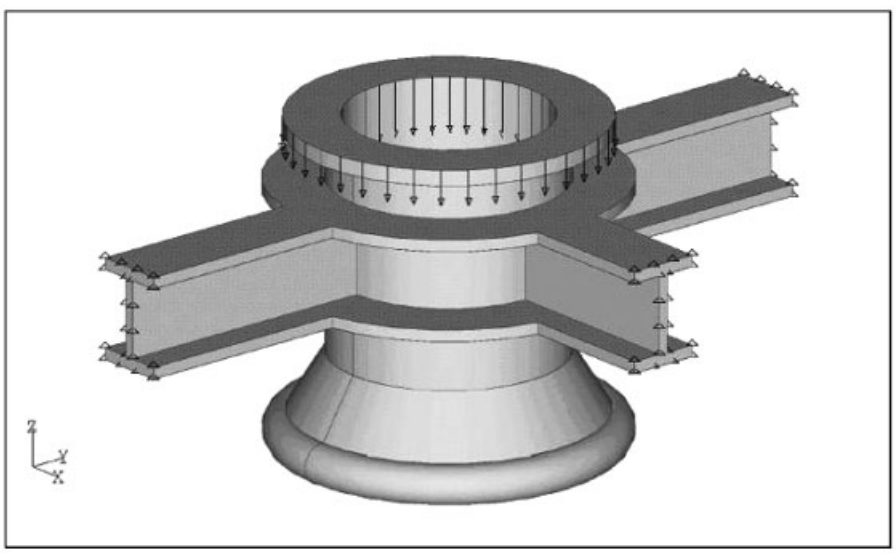

Figure 18. Simplified model of the three-dimensional riser connector.

DOI: 10.1002/nme

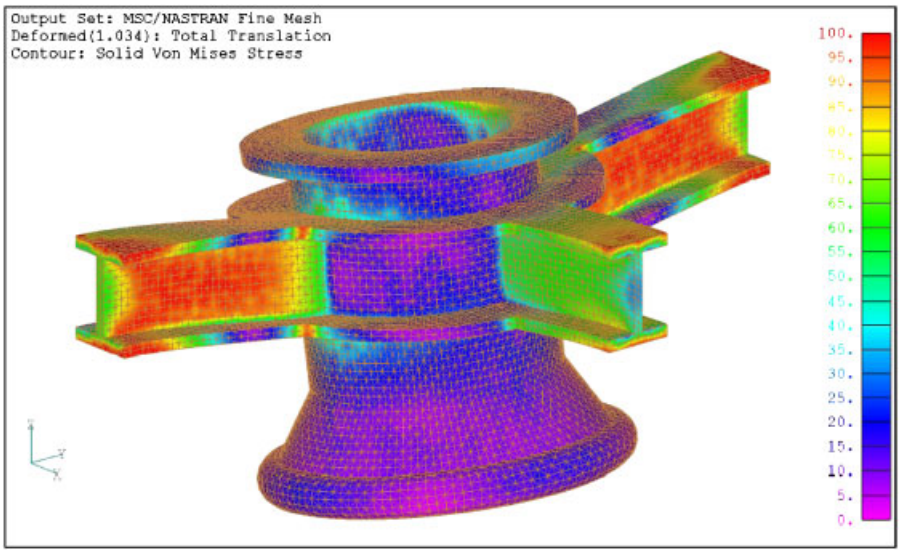

Figure 19. Reference solution of contour for elemental Von Mises stress obtained using FEM software (NASTRAN) *via* fine mesh.

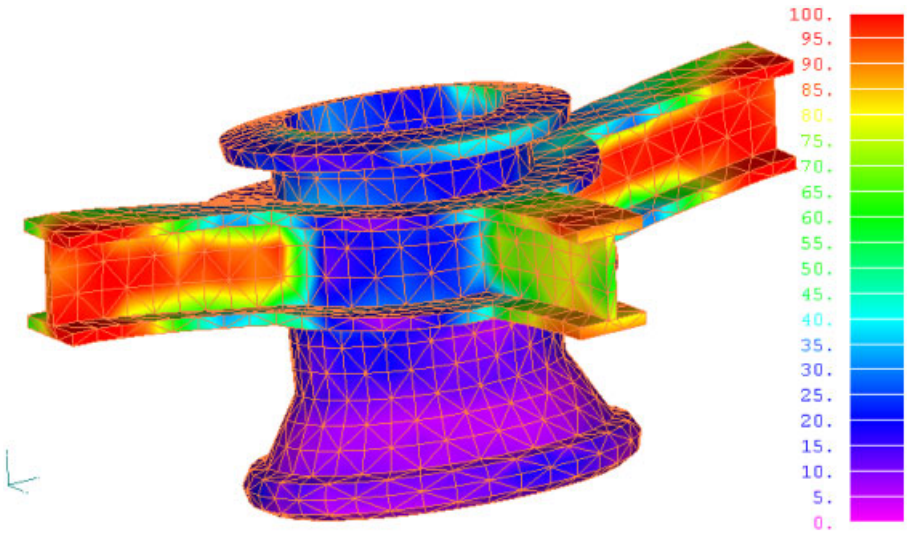

Figure 20. Contour of elemental Von Mises stress obtained using LC-PIM *via* coarse mesh.

of stress components of nodes located on the plane of $z = 0$ are plotted in the form of contour. Figures 15–17 show the comparison of stress contour between the reference solutions and the numerical ones for σ_{xx}, σ_{yy}, and τ_{xy}, respectively. It can be seen that the results obtained using the LC-PIM match well with the reference ones.

DOI: 10.1002/nme

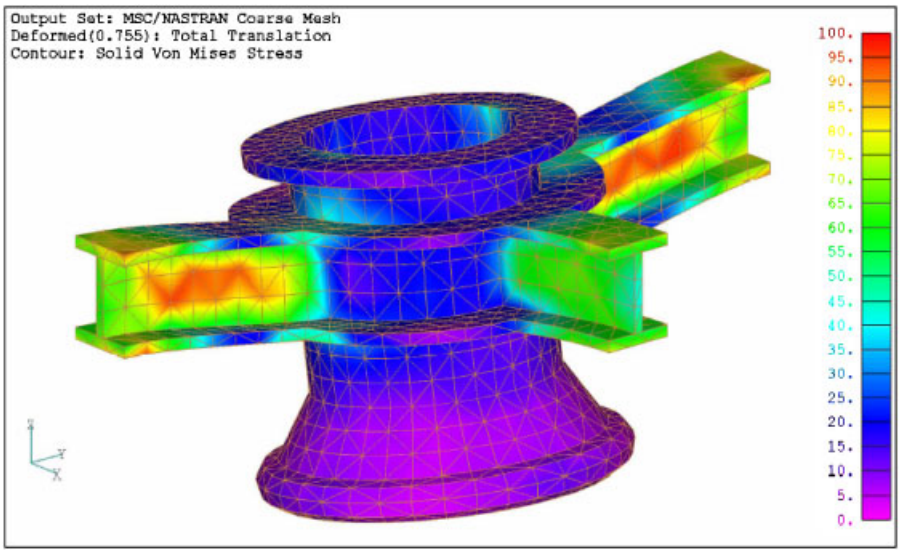

Figure 21. Contour of elemental Von Mises stress obtained using FEM *via* coarse mesh.

4.6. Riser connector

The following example comes from a real offshore project of Floating Production and Storage Unit (FPSO). Fluid transfer between FPSO and subsea pipeline is carried out through a kind of flexible pipe called riser, which is attached to FPSO shipside by riser connector. The simplified model of riser connector is shown in Figure 18 with the load being applied on the top flange of riser connector. The boundary conditions are defined at the end of I-beams where riser connector is supported by other structures. This riser connector is made of steel material with Young's modulus $E = 2.0 \times 10^5\,\mathrm{N/mm^2}$, Poisson's ratio $v = 0.32$.

Reference solution of this problem is obtained using the FEM software NASTRAN *via* very fine mesh (total 27 072 nodes), and the contour of elemental Von Mises stress is plotted in Figure 19 in the deformed shape of the riser connector. For the purpose of comparison, this problem is studied using both the present LC-PIM and the linear FEM *via* the same nodes distribution (total 2228 nodes). The numerical results of the elemental Von Mises stress got using these two methods are plotted in the form of contour are shown in Figures 20 and 21, respectively. It can be found that, although the riser connector is presented with less than one-tenth of the reference nodes distribution, the LC-PIM solution matches well with the reference one and is more close to it than that of the linear FEM.

5. CONCLUSIONS

In this work, the linearly conforming point interpolation method (LC-PIM) is formulated for 3-D problems. The present LC-PIM employs polynomial basis functions for field approximation and the shape functions so generated have the property of Kronecker delta function. Galerkin weak form is used and a stabilized nodal integration scheme with strain-smoothing technique is employed to perform the numerical integration. Some examples are studied numerically using the present method. Either for the benchmark problems which have the analytical solutions, or for the practical

DOI: 10.1002/nme

example with the complicated shapes, the LC-PIM can always obtain very stable and accurate results in terms of both displacements and stresses. The following remarks can be made:

- Shape functions are generated using the polynomial basis functions and have the property of Kronecker delta function, which allows straightforward imposition of point essential boundary conditions.
- With the implementation of strain-smoothing technique, the nodal integration scheme can obtain stable numerical results.
- Using the technique of strain smoothing, field gradients are computed directly using shape functions itself and no derivative of shape function is needed. This property can reduce the requirement on the smoothness of shape functions, which allows the LC-PIM to obtain accurate stress solutions, even using low-order shape functions.
- The present LC-PIM guarantees a linear exactness of the numerical solutions, which is also proven numerically by the standard patch test. This property ensures the stability and the convergence of the LC-PIM.
- Compared with the FEM using the linear tetrahedron element, the LC-PIM can achieve a higher accuracy and better efficiency.

REFERENCES

1. Lucy LB. A numerical approach to testing the fission hypothesis. *The Astronomical Journal* 1977; **8**(12): 1013–1024.
2. Liu GR, Liu MB. *Smoothed Particle Hydrodynamics—A Meshfree Practical Method*. World Scientific: Singapore, 2003.
3. Liszka T, Orkisz J. The finite difference methods at arbitrary irregular grids and its applications in applied mechanics. *Computers and Structures* 1980; **11**:83–95.
4. Nayroles B, Touzot G, Villon P. Generalizing the finite element method: diffuse approximation and diffuse elements. *Computational Mechanics* 1992; **10**:307–318.
5. Belytschko Y, Lu YY, Gu L. Element-free Galerkin methods. *International Journal for Numerical Methods in Engineering* 1994; **37**:229–256.
6. Liu WK, Jun S, Zhang YF. Reproducing kernel particle methods. *International Journal for Numerical Methods in Engineering* 1995; **20**:1081–1106.
7. Atluri SN, Zhu T. A new meshless local Petrov–Galerkin (MLPG) approach in computational mechanics. *Computational Mechanics* 1998; **22**:117–127.
8. Liu GR, Gu YT. A point interpolation method for two-dimensional solids. *International Journal for Numerical Methods in Engineering* 2001; **50**:937–951.
9. Liu GR. *Meshfree Methods*: *Moving Beyond the Finite Element Method*. CRC Press: Boca Raton, FL, 2002.
10. Liu GR, Gu YT. *An Introduction to Meshfree Methods and their Programming*. Springer: Dordrecht, The Netherlands, 2005.
11. Wang JG, Liu GR. A point interpolation meshless method based on radial basis functions. *International Journal for Numerical Methods in Engineering* 2002; **54**:1623–1648.
12. Liu GR, Zhang GY, Gu YT, Wang YY. A meshfree radial point interpolation method (RPIM) for three-dimensional solids. *Computational Mechanics* 2005; **36**(6):421–430.
13. Chen JS, Wu CT, Yoon S, You Y. A stabilized conforming nodal integration for Galerkin mesh-free methods. *International Journal for Numerical Methods in Engineering* 2001; **50**:435–466.
14. Liu GR, Zhang GY, Dai KY, Wang YY, Zhong ZH, Li GY, Han X. A linearly conforming point interpolation method (LC-PIM) for 2D solid mechanics problems. *International Journal of Computational Methods* 2005; **2**(4):645–665.
15. Liu GR, Li Y, Dai KY, Luan MT, Xue W. A linearly conforming RPIM for 2D solid mechanics. *International Journal of Computational Methods* 2006, in press.
16. Timoshenko SP, Goodier JN. *Theory of Elasticity* (3rd edn). McGraw-Hill: New York, 1970.
17. Zienkiewicz OC, Taylor RL. *The Finite Element Method* (5th edn). Butterworth Heinemann: Oxford, U.K., 2000.

DOI: 10.1002/nme